BEAM INSTRUMENTATION PERFORMANCE DURING COMMISSIONING OF THE ESS NORMAL CONDUCTING LINAC

I. Dolenc Kittelmann*, R. Baron, E. Bergman, E. Donegani, V. Grishin,
H. Hassanzadegan, H. Kocevar, N. Milas, R. Miyamoto, M. Mohammednezhad,
F. Nilen, D. Noll, K. Rosengren, T. Shea, R. Tarkeshian, C. Thomas
European Spallation Source ERIC, Lund, Sweden

Abstract

Once constructed, the European Spallation Source (ESS) will be a 5 MW pulsed neutron source based on a 2 GeV proton linac delivering 2.86 ms long pulses at a 14 Hz repetition rate. This paper focuses on the beam instrumentation performance during the recent linac beam commissioning up to drift tube linac (DTL) tank 4 with 74 MeV output energy. Instrumentation and measurement results will be presented for beam parameters such as current, position, energy, emittance and beam loss.

INTRODUCTION

The European Spallation Source (ESS) is a neutron-based research facility, currently under construction and designed to deliver the world's brightest neutron beams [1, 2]. The neutron production will be based on the bombardment of a tungsten target with a proton beam generated by a pulsed linac. The linac will accelerate and transport the protons towards the target through a normal-conducting (NCL) and superconducting (SCL) linac (Fig. 1) resulting in a beam with a peak current of 62.5 mA, 2.86 ms pulse length, 14 Hz repetition rate, and energy of 2 GeV once the linac design average power of 5 MW is reached.

For a high-power machine like the ESS linac, one of the biggest challenges during its commissioning and operations is to minimize beam losses and protect its components by adequately adjusting the electromagnetic elements and achieving ideal beam parameters. A comprehensive set of proton beam instrumentation has been developed to provide detailed beam property measurements throughout the linac and thus to support achieving the required beam parameters. The set comprises instruments for beam characterisation along the linac to provide beam profile, position, energy, current and loss measurements [3].

The ESS linac commissioning is performed in phases. Each commissioning phase is focused on the linac parts up to the selected beam destination. In parallel, the linac installation downstream of the end-destination continues. Three commissioning phases have been completed successfully with low power beam and end-destinations in LEBT (2018-2019) [4, 5], in MEBT (2021-2022) [6] and at the end of DTL1 reaching 21 MeV (2022) [7–9]. From April to July 2023, the commissioning has advanced to the fourth phase, reaching the end of the DTL4 tank with an output energy of 74 MeV. Towards the end of 2024, the beam commissioning

will continue to the Dump, while the first beam on target is planned to be achieved at the end of 2025 followed by the start of the user program in 2026.

This paper focuses on ESS beam instrumentation deployed for the DTL4 commissioning phase and highlights their key features and contributions during this phase.

BEAM INSTRUMENTATION FOR THE NCL COMMISSIONING

The ESS beam instrumentation is being deployed in a staged approach. Systems that are critical for meeting commissioning goals proceed through a formal verification process beginning with unit testing in the laboratory followed by integrated system testing, and finally, formal testing with beam to achieve operational status. Figure 1 summarises the instrumentation systems installed for the DTL4 commissioning run. The Faraday Cups (FCs), Beam Current Monitor (BCM), and Beam Position Monitor (BPM) have all gone through the aforementioned formal verification workflow. In addition, several other systems, at an intermediate stage of their development were deployed for diagnostic beam studies to gain early operational experience. The Wire Scanners (WSs) [10], Emittance Measurement Unit (EMU) [7] and two types of Beam Loss Monitors (BLMs) were deployed at this level. Beam studies with the neutron-sensitive BLM (nBLM) and horizontal EMU station offered valuable data for system development as well as beam characterisation and the results are presented here together with results with the FCs, BPM and BCM systems. In addition, some limited beam studies were performed with WSs, the vertical EMU station and the Ionisation Chamber based BLM [11] system. Results from these systems will be covered in future publications.

Faraday Cups

Three Faraday cups were operational during the DTL4 commissioning. Once inserted, each FC is a beam end-destination and measures the transported beam current at the destination. The FC locations were in the LEBT [5, 12], in the MEBT [12, 13] and in a dedicated shielding at the (foreseen) position of DTL5 [12, 14] tank. All FCs are water-cooled and rely on a pneumatic actuator to move in or out of the beamline.

The LEBT FC is designed to withstand full power at the ion source exit, namely 75 keV proton beam pulses with up to 100 mA current, 6 ms pulse length at 14 Hz repetition rate. However, MEBT and DTL4 FC can cope with only
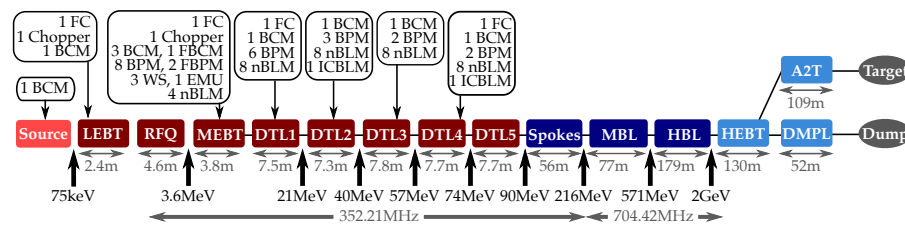
* Irena.DolencKittelmann@ess.eu

Figure 1: ESS linac: the normal-conducting linac (NCL, in red) is composed of an ion source, Radio Frequency Quadrupole (RFQ), Drift Tube Linac (DTL) with five tanks, Low Energy (LEBT) and Medium Energy Beam Transport (MEBT) sections. Spoke, Medium Beta (MBL) and High Beta (HBL) Linac constitute the Superconducting Linac (SCL, in dark blue). Beam transport and delivery to Target and tuning Dump consist of High Energy Beam Transport (HEBT) line, Accelerator-to-Target (A2T) line and the dump line (DMPL). Beam instrumentation and choppers used in the 2023 commissioning run are indicated.

reduced beam power. The MEBT FC supported commissioning activities with 3.6 MeV beam and current up to nominal 62.5 mA with up to 5 µs or 50 µs pulse length at 14 Hz or 1 Hz repetition rate, respectively. When the destination was the DTL4 FC, the beam parameters envelop was set to allow commissioning studies with low (up to 6 mA) beam current up to 50 µs pulse length and up to 14 Hz repetition rate or high beam current (up to 62.5 mA) up to either 5 µs or 50 µs pulse length and 1 Hz or 0.2 Hz repetition rate, respectively. Restrictions were set on the allowed energy range at the DTL4 FC location (i.e. required acceleration in consecutive tanks) depending on particular sets of beam parameter limits.

At the end of the commissioning and after four weeks of radioactive decay, the residual dose rate of approximately 1 mSv/h in the vicinity of the DTL4 FC allowed the removal the DTL4 FC to leave space for installing the DTL5 tank. During the next commissioning phase and the years to come of operation of the ESS accelerator, there will be four FCs permanently installed in the NCL: one in the LEBT, one in the MEBT, one in the DTL2 intertank and one in the DTL4 intertank.

Beam Current Monitors

Nine Beam Current Monitors were successfully used during the DTL4 beam commissioning phase [15]. Most of these sensors are custom-designed by Bergoz to meet the ESS requirements, including the beam pipe dimensions, magnetic shielding and protection for the BCM ceramic.

The analogue signal from each BCM sensor is first buffered and amplified in a wall-mount Front End (FE) unit and then filtered and further processed in a custom-designed Back End (BE) in the BCM rack. The signal is then converted to digital and FPGA processed to provide the required beam monitoring and machine protection functions.

The BCMs allowed beam current measurement with 0.1 mA accuracy and with a noise level lower than 50 µA peak-to-peak and bandwidth of 1 MHz. The measurements included pulse profile, average beam current over a region of interest (ROI) and pulse charge with each BCM. These measurements also aided the machine operators in identifying electrons from the cavities due to multipacting and RF/vac-

uum breakdowns (Fig. 2) as well as the (expected) scattered beam from the MEBT chopper dump (Fig. 3). Given that the BCM is located directly after the MEBT chopper dump while the other beam measurement devices, such as the BPMs and the FCs, are located further downstream, the scattered beam could only be measured by this BCM due to the geometrical constraints.

The BCM system further provided a precise measurement of the width, repetition rate and arrival time of the beam trigger for consistency checks, thus avoiding unexpected beams due to human errors and/or timing system-related issues.

A post-mortem ring buffer was implemented in the BCM firmware to capture BCM data upon a beam trip. It proved to be a very effective tool for trip analysis and improvements in beam availability. Furthermore, differential interlocks with several BCM pairs were verified with beam and used for beam loss measurement and machine protection.

A BCM channel with a modified beam trigger was successfully tested and verified for 1-hour average beam current measurements with accuracy better than 1 µA.

Figure 2 shows a low current beam pulse measured by seven BCMs from the LEBT to the DTL tank4. Figure 3 shows an example of the pulse width reduction and scattered beam, both caused by the MEBT chopper.

A complete suite of protection functions was used to detect whether, among others, the amplitude, width and repetition rate of the beam pulse were outside the allowed limits and ensure their consistency with the selected beam mode. It included several thresholds that were configured by the BCM firmware based on the selected beam mode and destination. The thresholds were chosen to be consistent with the predefined sets of envelopes. However, some adjustments were made in the configuration of the protection functions based on a beam damage assessment. These were mainly to address beam availability issues due to RF breakdowns and other disturbances originating from the cavities [15].

Beam Position and Phase Monitors

Beam position and phase monitors have been extensively used in this commissioning to characterise the proton beam properties. Beam studies including trajectory correction,
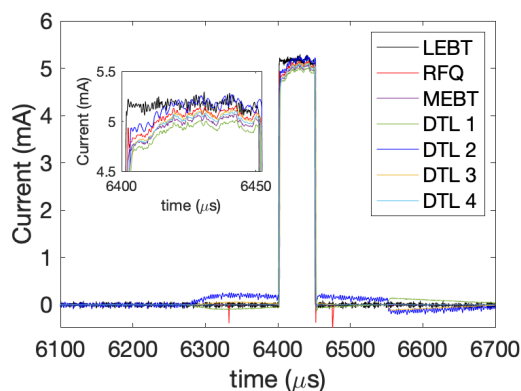
Figure 2: ESS beam pulse as measured with the LEBT, RFQ, MEBT, DTL1 and DTL4 BCMs. The negative spikes on the RFQ BCM readout (red) are due to multipacting, and the small changes in the baseline level with the DTL2 BCM (blue) are due to the field emission from the cavities.
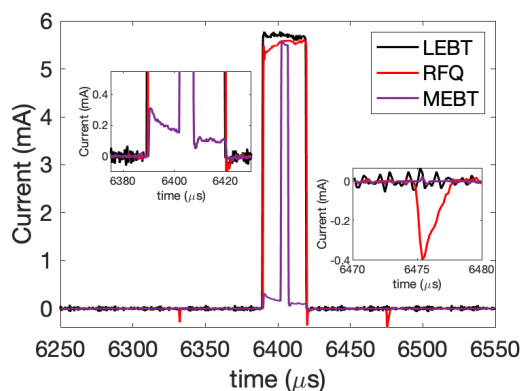

Figure 3: Beam pulses from the LEBT (black), RFQ (red) and MEBT BCM located in the middle of MEBT after the chopper dump (violet). The none-zero floor of MEBT BCM waveform is due to the scattered beam from the MEBT chopper dump.

RF phase scans, longitudinal pulse shape tuning and beam timing characterisation, have been performed based on the data provided by the 21 BPMs in operation during the DTL4 commissioning phase.

The ESS BPM system has several FPGA-based processing channels delivering data in EPICS Process Variables. Data streams for individual antenna's raw data, at approximately 20 MHz bandwidth and 88 MSa/s are available, as well as near-IQ waveforms for positions, magnitudes and beam phase measurements. Typical waveforms for positions and phases are measured at a rate of approximately 5.8 MHz with a bandwidth around 2 MHz [16]. Scalars for averaged data are also calculated at a rate of 1 value per beam pulse in a ROI determined by timing events. BPM waveforms have proven crucial in understanding and adjusting the parameters of the machine to optimize uniformity in pulse characteristics within a pulse and timing characterisations of the beam.

The RF system in NCL operates at 352.21 MHz while the BPMs were designed to operate at the 704.4 MHz second harmonic in order to minimise the interference across the systems. The RF processing chain of the BPM signals and data have been standardized for all the BPMs.

Eight MEBT BPMs were designed based on matched stripline sensors [17] and installed in the machine.

Thirteen DTL BPMs were designed based on shorted stripline sensors and commissioned in DTL tanks 1, 2, 3 and 4. Interference between BPMs and RF system was more strongly observed in the DTL1, but has been addressed during the commissioning. In some locations inside the DTL tanks, where the drift tubes are close to the RF ports, the RF system couples strongly to the second harmonic, which then leaks to the BPM sensors near the RF ports interfering with the beam signal excited on the BPM striplines. Additional RF high-pass filters were introduced on the BPM inputs to filter the first harmonic that couples into the BPM striplines.

Reported BPM measurements during a typical phase scan are presented in Fig. 4. During the phase scan, the set-point of the RF cavity phase under test is plotted together with the phase of the signals measured by BPMs. The measured amplitude of the BPM signals also changes as a function of the cavity RF phase set-point since the bunch length varies with the cavity RF phase and is also presented in the same plot.
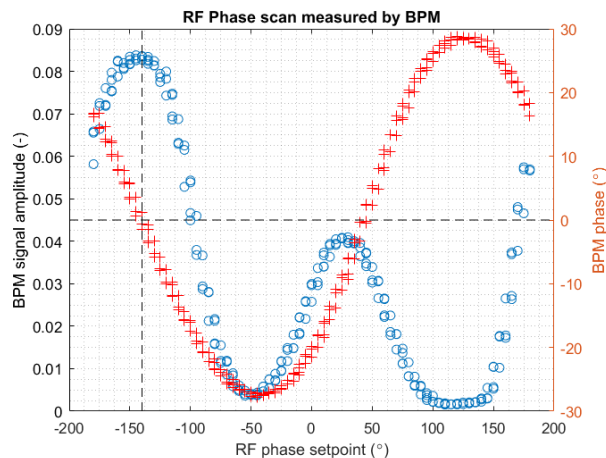

Figure 4: Typical phase scan measurements performed by a downstream MEBT BPM during a phase scan. BPM amplitude and BPM phase are shown on the plot as a function of the RF phase of MEBT buncher 1.

Beam studies slots during the DTL4 commissioning run were assigned to long-term stability measurements of the beam characteristics, and the BPM phase and amplitude measurements are reported in Fig. 5.

Emittance Measurement Unit

The MEBT EMU is a slit-grid type with a grid located 368 mm downstream of a slit with 100 µm aperture. The grid consists of 24 tungsten wires of 35 µm diameter mounted with a pitch of 0.5 mm. Signals are generated by secondary
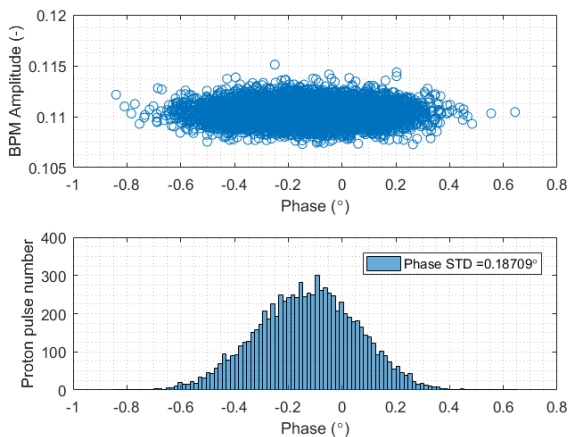
Figure 5: Stability measurements of the beam phase and amplitude recorded with one of the BPMs in MEBT over 4 hours of operation with a 6 mA and 5 µs beam.

Figure 6: Emittance figure after baseline subtraction with 1 kV bias voltage applied.

electron emission and acquired by configurable gain stages followed by 5 MSa/s digitisers. The grid PCB is surrounded by bias plates that can be biased up to ± 1.2 kV to control the electric field experienced by the electrons. The tungsten wires mounted on the bias plates enhance the field created by the plates.

The instrument commissioning activities focused on signal quality investigations and some initial beam studies. Measurements without bias show significant negative signals from secondary electrons picked up on wires adjacent to those exposed to the beam. When biased sufficiently (>500 V), these negative signals are suppressed. At the same time, due to the effective emission of secondary electrons, the positive signal on the exposed wires is enhanced by approximately a factor of 4.

Figure 6 shows an example of a scanning result in the horizontal plane with 167 µm resolution, taking multiple acquisitions of the grid signals with the grid position shifted by 0/3, 1/3 and 2/3 of the wire pitch to improve angular resolution. The signal is integrated over the final 15 µs of the 30 µs long beam used for measurement. The first 15 µs shows varying emittance, likely from space charge compensation in the LEBT. The background extending across the entire range of measured x' is a suspected result of beam scattering from the slit aperture. It was found to follow a Gaussian function and can be subtracted. A preliminary analysis shows an RMS emittance consistent with the beam physics model.

Beam Loss Monitors

Two types of BLM systems differing in detector technology have been conceived at ESS. The nBLM [18] is based on 82 neutron detectors primarily covering the lower energy part of the ESS linac. Conversely, the ICBLM [11] consists of 266 ionisation chambers [19], located predominantly in the high energy parts of the ESS linac.

The ESS nBLM system is based on neutron-sensitive Micromegas devices, specially designed for the lower energy
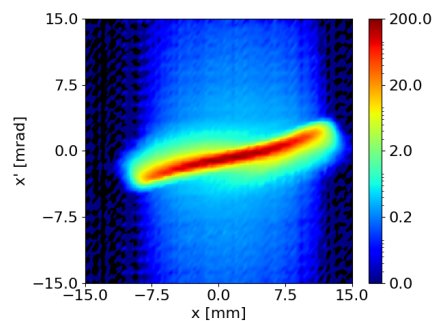
part of the ESS linac [20]. Two types of nBLM detectors with complementary functionality have been developed. Fast detectors (nBLM-F) are designed to detect fast losses in accidental scenarios when high particle fluxes are expected. On the other hand, slow detectors (nBLM-S) primarily aim to monitor losses with low particle fluxes. The nBLM system is designed to discriminate beam loss–induced fast neutrons from the background (RF-induced photons, background slow neutrons) on an event-by-event basis. It is achieved by continuous real-time FPGA-based data processing of digitised raw signal sampled at 250 MHz from each nBLM detector, resulting in fully processed data streams for monitoring and machine protection purposes. Additionally, detailed data at various stages of data processing are being buffered and can be retrieved on demand.

During the previous two commissioning phases, the nBLM system underwent initial deployment and first studies with ESS beam. In 2023, the system installation advanced to take part in studies during the DTL4 commissioning run with 36 nBLM detectors covering MEBT and the first four DTL tanks. Detailed data holding information about interesting events (neutron, noise or background events) and monitoring data have been continuously recorded for two weeks. Furthermore, several dedicated experiments with stable beam conditions were performed where a selected set of beam parameters was kept unchanged for ≈30 min. All data taken during this commissioning period is currently being analysed offline in order to study the system response, explore the background and noise environment and develop a procedure for setting the system configuration. An example of extracted information is shown in Fig. 7 representing a distribution of neutron events over time in machine cycle recorded with one of the nBLM-F detectors. The plot demonstrates a 50 µs and 5 µs beam pulse starting at ~6.5 ms. Figure 8 summarises preliminary results on the number of neutron events (single neutron or pile-up) per beam pulse recorded with nBLM detectors during a set of time periods with different beam currents and pulse lengths. For the fast detectors the observed peaks at end of DTL3 and DTL4 are found to be consistent with the observations from activation surveys. The peak at the end of DTL1 could be qualitatively explained with the simulation results [21] indicating that
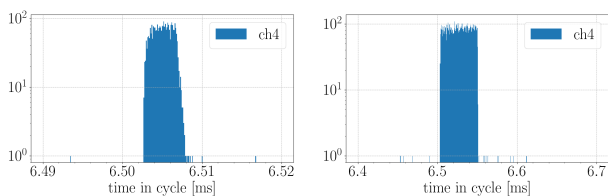
Figure 7: Distribution of neutron events over time in cycle recorded with one of the nBLM-F detectors during a ~2 hour and ~2.5 hour time window with a 5 µs (left) and 50 µs (right) long beam pulse, respectively.

majority of particles outside of the DTL1 acceptance are expected to be lost at this location. Note that, for slow detectors, the event rate differs from the actual neutron rate due to pile-up. Further analysis is ongoing in order to account for that.
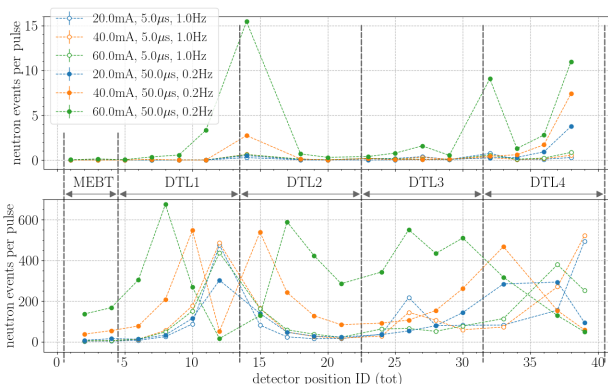

Figure 8: Preliminary results of number of neutron events recorded with fast (top) and slow (bottom) nBLM detectors for different beam parameters.

Bunch-by-bunch Characterization

The Fast BPM (FBPM) and Fast BCM (FBCM) systems provide high bandwidth and high sampling rate measurements for bunch-by-bunch characterisation of the beam. The FBCM, with 700 MHz bandwidth is based on a Bergoz Fast Current Transformer and a 20 GSa/s acquisition system. The Fast BPM is based on two regular stripline BPMs, positioned 30.1 cm apart, with separate 20 GSa/s acquisition systems each incorporating 3 GHz analog front-end electronics. Propagation delays between the FBPM channels are matched to ± 50 ps resulting in an energy measurement accuracy of ± 20 keV with a precision of ± 100 keV [7]. The FBCM and FBPM were both used to verify LEBT and MEBT chopper rise and fall times and for precise timing alignment of the two choppers.

When a protection function identifies unacceptable beam conditions, the Fast Beam Interlock System (FBIS) [22] utilizes several actuators to inhibit beam production. These actuators include the LEBT and MEBT choppers that dump the beam that is already propagating through the front end of the linac. Under controlled test conditions, the FBPM sys-

tem characterised the reaction time of the complete interlock chain. For this test, a fault was instigated by lowering the maximum current threshold in the MEBT BCM system located just after the MEBT chopper. The full interlock chain consists of the BCM system, signal transmission, FBIS processing, signal transmission to the choppers and the chopper systems themselves. When the MEBT chopper was used, the measured reaction time was approximately 2.3 µs (Fig. 9) and when only the LEBT chopper was used, the measured reaction time was approximately 3.2 µs. The reaction time difference between the two cases is due to the beam propagation time between the LEBT chopper and MEBT chopper.
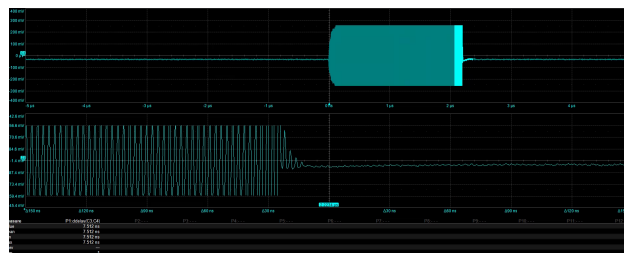

Figure 9: Full chain interlock reaction time measured by the fast BPM with both LEBT and MEBT chopper included in the systems for inhibiting beam production.

CONCLUDING REMARKS

The primary role of the NCL at this phase of the ESS project is to provide an appropriate beam for the commissioning of the remaining accelerator. As evidenced in the preceding sections, the NCL beam instrumentation systems supported the NCL commissioning and are ready to support the upcoming campaigns: 1. initial commissioning of the entire SCL and the beam transport line to the linac Dump and 2. first beam on target by transporting beam through the dogleg and A2T beam delivery system.

In parallel with the NCL commissioning activities, the diagnostics team continued to install SCL and transport line instrumentation. Downstream of DTL4, the instrumentation suite will include an additional 10 BCMs, 77 BPMs, 46 nBLMs, 262 ICBLMs, 5 pairs of Ionisation Profile Monitors [23], 9 pairs of WSs in SCL and A2T, 3 pairs of Fast Wire scanners in the HEBT, 3 Imaging systems [24, 25] and 4 Aperture Monitors [26].

ACKNOWLEDGEMENTS

The authors wish to thank to all past and present colleagues from ESS and external institutes who contributed to the ESS linac project. In particular, we appreciate the critical support received during the design, development, manufacturing, installation and testing of the BI systems.

REFERENCES

[1] S. Peggs *et al.*, "ESS technical design report," ESS ERIC, Tech. Rep. ESS-DOC-274, 2013. http://eval.esss.lu.se/cgi-bin/public/DocDB/ShowDocument?docid=274

[2] R. Garoby *et al.*, "The European Spallation Source design," *Phys. Scr.*, vol. 93, no. 1, p. 014 001, 2018. doi:10.1088/1402-4896/aa9bff

[3] T. Shea *et al.*, "Overview and Status of Diagnostics for the ESS Project," in *Proc. of International Beam Instrumentation Conference (IBIC'17)*, Grand Rapids, MI, USA, 2018, paper MO2AB2, pp. 8–15. doi:10.18429/JACoW-IBIC2017-MO2AB2

[4] C. Derrez *et al.*, "Initial Performance of the Beam Instrumentation for the ESS IS & LEBT," in *Proc. 10th International Particle Accelerator Conference (IPAC'19)*, Melbourne, Australia, 2019, paper WEPGW076, pp. 2650–2653. doi:10.18429/JACoW-IPAC2019-WEPGW076

[5] N. Milas *et al.*, "Commissioning of the ESS Front End," in *Proc. HB'21*, Batavia, IL, USA, 2022, paper THDC2, pp. 225–230. doi:10.18429/JACoW-HB2021-THDC2

[6] N. Milas *et al.*, "Beam Tuning Studies in the ESS MEBT," in *Proc. 11th Int. Beam Instrum. Conf. (IBIC'22)*, Kraków, Poland, 2022, paper MO2C2, pp. 6–10. doi:10.18429/JACoW-IBIC2022-MO2C2

[7] T. Shea *et al.*, "Beam Instrumentation Performance During Commissioning of the ESS RFQ, MEBT and DTL," in *Proc. 11th Int. Beam Instrum. Conf. (IBIC'22)*, Kraków, Poland, 2022, paper MOP07, pp. 32–36. doi:10.18429/JACoW-IBIC2022-MOP07

[8] R. Miyamoto *et al.*, "Beam Commissioning of Normal Conducting Part and Status of ESS Project," in *Proc. 31st International Linear Accelerator Conference (LINAC'22)*, Liverpool, UK, 2022, paper MO1PA02, pp. 18–24. doi:10.18429/JACoW-LINAC2022-MO1PA02

[9] D. C. Plostinar *et al.*, "Status of the Normal Conducting Linac at the European Spallation Source," in *Proc. IPAC'22*, Bangkok, Thailand, 2022, paper WEPOTK001, pp. 2019–2022. doi:10.18429/JACoW-IPAC2022-WEPOTK001

[10] C. Derrez *et al.*, "Wire Scanner Systems at the European Spallation Source (ESS): Tests and First Beam Commissioning Results," in *Proc. 31st International Linear Accelerator Conference (LINAC'22)*, Liverpool, UK, 2022, paper TUPOJO13, pp. 372–375. doi:10.18429/JACoW-LINAC2022-TUPOJO13

[11] I. D. Kittelmann *et al.*, "Ionisation Chamber Based Beam Loss Monitoring System for the ESS Linac," in *Proc. 8th International Beam Instrumentation Conference (IBIC'19)*, Malmö, Sweden, 2019, paper MOPP023, pp. 136–140. doi:10.18429/JACoW-IBIC2019-MOPP023

[12] E. Donegani, I. Bustinduy, C. Derrez, T. Grandsaert, A. R. Páramo, and T. Shea, "Status of the Faraday Cups for the ESS linac," in *Proc. IBIC'19*, Malmö, Sweden, 2019, paper MOPP044, pp. 205–208. doi:10.18429/JACoW-IBIC2019-MOPP044

[13] A. R. Páramo *et al.*, "Design of the ESS MEBT Faraday Cup," in *Proc. IBIC'19*, Malmö, Sweden, 2019, paper MOPP014, pp. 106–110. doi:10.18429/JACoW-IBIC2019-MOPP014

[14] E. L. B. Cheymol, "Conceptual Design of the ESS DTL Faraday Cup," in *Proc. LINAC 2014*, Geneva, Switzerland, paper MOPP037, pp. 140–142.

[15] H. Hassanzadegan *et al.*, ""BCM System Optimization for ESS Beam Commissioning through the DTL Tank4"," in *Proc. 12th Int. Beam Instrum. Conf. (IBIC'23)*, Saskatoon, Saskatchewan, Canada, 2023, this conference, paper TUP038.

[16] R. Baron *et al.*, "ESS Beam Position and Phase Monitor System," in *Proc. IBIC'19*, Malmö, Sweden, 2019, pp. 543–547. doi:10.18429/JACoW-IBIC2019-WEPP015

[17] S. Varnasseri *et al.*, "Design and fabrication of stripline bpm for the ess mebt," *NIMA*, vol. 987, p. 164 835, 2021. doi:10.1016/j.nima.2020.164835

[18] I. Dolenc Kittelmann *et al.*, "Neutron sensitive beam loss monitoring system for the european spallation source linac," *Phys. Rev. Accel. Beams*, vol. 25, no. 2, p. 022 802, 2022. doi:10.1103/PhysRevAccelBeams.25.022802

[19] I. D. Kittelmann and V. Grishin, "Detector response studies of the ESS Ionization Chamber," in *Proc. 12th Int. Beam Instrum. Conf. (IBIC'23)*, Saskatoon, Saskatchewan, Canada, 2023, paper TUP004, this conference.

[20] L. Segui *et al.*, "Detector design and performance tests of the ess-neutron beam loss monitor detectors," *JINST*, vol. 18, no. 01, P01013, 2023. doi:10.1088/1748-0221/18/01/P01013

[21] Y. Levinsen *et al.*, "Beam Dynamics Challenges in the ESS Linac," in *Proc. of ICFA Advanced Beam Dynamics Workshop on High-Intensity and High-Brightness Hadron Beams (HB'16)*, Malmö, Sweden, 2016, paper TUAM3Y01, pp. 315–318. doi:10.18429/JACoW-HB2016-TUAM3Y01

[22] S. Gabourin *et al.*, "The ESS Fast Beam Interlock System: First Experience of Operating With Proton Beam," in *Proc. LINAC'22*, Liverpool, UK, 2022, paper MOPORI17, pp. 265–267. doi:10.18429/JACoW-LINAC2022-MOPORI17

[23] J.Marroncle *et al.*, "Non-Invasive Profiles for the cold linac part of the ESS accelerator," in *Proc. 12th Int. Beam Instrum. Conf. (IBIC'23)*, Saskatoon, Saskatchewan, 2023, paper TUPD36, this conference.

[24] C. A. Thomas *et al.*, "Preliminary Measurement on Potential Luminescent Coating Material for the ESS Target Imaging Systems," in *Proc. IBIC'16*, Barcelona, Spain, Sep. 2016, paper TUPG82, pp. 559–562. doi:10.18429/JACoW-IBIC2016-TUPG82

[25] E. Adli *et al.*, "Progress of the ESS Proton Beam Imaging Systems," in *Proc. LINAC'22*, Liverpool, UK, 2022, paper TUPOJO20, pp. 394–397. doi:10.18429/JACoW-LINAC2022-TUPOJO20

[26] C. Thomas *et al.*, "J-PARC Test of ESS Beam on Target Diagnostics Prototypes Aperture Monitor and GRID," in *Proc. IBIC'19*, Malmö, Sweden, 2019, paper TUPP032, pp. 387–391. doi:10.18429/JACoW-IBIC2019-TUPP032